

- Loneragan, in *Iron and Related Transition Metals in Microbial Metabolism*, G. Winokelman, C. J. Carrano, Eds. (Harwood Academic, Netherlands, 1997), pp. 187–215.
15. Putative c-type cytochromes were identified using the cytochrome c heme-binding signature family motif as given in Prosite (PS00190) (www.expasy.ch).
 16. Sequence data for the completed *Desulfovibrio vulgaris* genome were produced by The Institute for Genomic Research (TIGR) (www.tigr.org).
 17. F. Caccavo Jr. et al., *Appl. Environ. Microbiol.* **60**, 3752 (1994).
 18. H. Cypionka, *Annu. Rev. Microbiol.* **54**, 827 (2000).
 19. R. S. Lemos et al., *FEBS Lett.* **496**, 40 (2001).
 20. T. A. Dailey, H. A. Dailey, *J. Biol. Chem.* **273**, 13658 (1998).
 21. M. Lehmann, B. Tshisuaka, S. Fetzner, F. Lingens, *J. Biol. Chem.* **270**, 14420 (1995).
 22. B. L. Taylor, I. B. Zhulin, *Microbiol. Mol. Biol. Rev.* **63**, 479 (1999).
 23. C. Thelwell, N. J. Robinson, J. S. Turner-Cavet, *Proc. Natl. Acad. Sci. U.S.A.* **95**, 10728 (1998).
 24. H. Tsujibo, K. Miyamoto, T. Okamoto, H. Orikoshi, Y. Inamori, *Appl. Environ. Microbiol.* **66**, 3778 (2000).
 25. J. R. Kirby, D. R. Zusman, *Proc. Natl. Acad. Sci. U.S.A.* **100**, 2008 (2003).
 26. The GenBank accession number of the *G. sulfurreducens* chromosome is AE017180.
 27. Funded by the U.S. Department of Energy's Office of Science, Office of Biological and Environmental Research, and Natural and Accelerated Bioremediation Research and Microbial Genomes Programs. We

thank M. Heaney, S. Lo, M. Holmes, B. Lee, C. Irwin, R. Karamchedu, and V. Sapiro for database and information technology support at TIGR; the TIGR faculty and sequencing core for expert advice and assistance; and A. Kwamena-Poh for assistance in the preparation of this manuscript.

Supporting Online Material

www.sciencemag.org/cgi/content/full/302/5652/1967/DC1

Materials and Methods

SOM Text

Figs. S1 to S5

Tables S1 to S6

References

3 July 2003; accepted 14 October 2003

Crystal Structure of the RC-LH1 Core Complex from *Rhodopseudomonas palustris*

Aleksander W. Roszak,¹ Tina D. Howard,² June Southall,² Alastair T. Gardiner,² Christopher J. Law,² Neil W. Isaacs,^{1*} Richard J. Cogdell^{2*}

The crystal structure at 4.8 angstrom resolution of the reaction center–light harvesting 1 (RC–LH1) core complex from *Rhodopseudomonas palustris* shows the reaction center surrounded by an oval LH1 complex that consists of 15 pairs of transmembrane helical α - and β -apoproteins and their coordinated bacteriochlorophylls. Complete closure of the RC by the LH1 is prevented by a single transmembrane helix, out of register with the array of inner LH1 α -apoproteins. This break, located next to the binding site in the reaction center for the secondary electron acceptor ubiquinone (UQ_B), may provide a portal through which UQ_B can transfer electrons to cytochrome b/c₁.

Photosynthesis is one of the most important biological reactions on Earth. It provides all of the oxygen we breathe and, ultimately, all the food we eat. Purple photosynthetic bacteria have proved to be excellent model systems in which to study the light reactions of photosynthesis. Their light reactions usually begin with the absorption of a photon by the light harvesting (LH) or antenna system (1). This absorbed energy is then rapidly and efficiently transferred to the reaction center (RC), where it is used to initiate cyclic electron transport between the RC, cytochrome b/c₁, and cytochrome c (Fig. 1), producing a proton gradient that drives adenosine triphosphate (ATP) synthase and ultimately converts solar energy into useful chemical energy. These reactions take place in the photosynthetic membrane, where the RC is surrounded by two types of antenna complexes, called LH1

and LH2 (2). The LH1 antenna forms a stoichiometric complex with the RC, called the RC-LH1 core complex. Both types of LH complexes are constructed on the same modular principle. Bacteriochlorophyll *a* (Bchl_a) and carotenoids are noncovalently bound to two types of low molecular weight (5 to 7 kD), hydrophobic apoproteins, called α and β , each of which has a single membrane-spanning α helix. The functioning LH complexes are oligomers of these $\alpha\beta$ pairs, together with their associated pigments (2).

In the past few years, structural analysis of some of these pigment-protein complexes has substantially advanced the field. The structure of the purple bacterial RC was determined in 1985 (3) and is now known to a resolution of better than 2 Å (4). The structure of the LH2 complex from the purple bacterium *Rhodopseudomonas acidophila* was determined in 1995 (5), and it is now also at 2 Å resolution (6). LH2 has a nonameric ring structure. Nine α -apoproteins form an inner ring of α helices, while nine β -apoproteins form an outer ring of α helices. The Bchl_a and carotenoid molecules are located between these two cylinders of α helices. The ATP synthase (7)

and cytochrome b/c₁ (8) complex structures from bovine heart mitochondria have also been determined, to resolutions of 2.8 and 3.0 Å, respectively.

The structure of the LH1 complex has been investigated previously by electron cryomicroscopy on two-dimensional (2D) crystals. An 8.5 Å resolution projection map of a reconstituted LH1 complex from *Rhodospirillum rubrum* (9) revealed a large ($\alpha\beta$)₁₆ cyclic structure with features similar to LH2 and in which the “hole” in the middle was sufficient to accommodate an RC. Similar projection maps of RC-LH1 core complexes from several species of purple bacteria (*R. rubrum*, *Rhodobacter sphaeroides*, and *Rps. acidophila*) have confirmed that the RC is located within the LH1 ring (10–13). However, some studies have questioned whether, when the RC is present, the LH1 ring is actually complete (14).

Figure 1 shows a flow of electrons from the RC to the cytochrome b/c₁ complex through the fully reduced ubiquinone UQ_BH₂ (ubiquinol), which is generally thought to migrate from the RC into the membrane (15). Models in which the RC is completely surrounded by a double palisade of LH1 α helices raise the question of how UQ_BH₂ could escape from the core complex into the membrane (16). Two species of purple bacteria, *Rb. sphaeroides* and *Rb. capsulatus*, have a gene called *pufX* that appears to play a role in this process (17, 18). When the PufX protein is present, reduced and oxidized ubiquinones can rapidly shuttle between the RC and the cytochrome b/c₁ complex (19, 20). However, if this gene is deleted, the bacteria will grow photosynthetically only when LH1 is also deleted or modified so that full-size complexes are not formed (21–23). It has been suggested therefore that the PufX protein forms a gate in the LH1 ring through which the UQ can exchange (16).

We determined the crystal structure of the RC-LH1 core complex from the purple bacterium *Rhodopseudomonas palustris* at 4.8 Å resolution (24). Initial phases at 4.8 Å were calculated by the molecular replacement (MR) method with the RC from *Rb. spha-*

¹Department of Chemistry, ²Division of Biochemistry and Molecular Biology, Institute of Biomedical and Life Sciences, University of Glasgow, Glasgow G12 8QQ, UK

*To whom correspondence should be addressed. Email: r.cogdell@bio.gla.ac.uk (R.J.C.) or n.isaacs@chem.gla.ac.uk (N.W.I.)

REPORTS

eroides (25) as a model. Figure 2A shows the ($2mF_o - DF_c$) error-weighted electron density map calculated after rigid-body refinement of the best MR solution. This map clearly shows electron density located outside and around the RC. The LH1 α helices and bacteriochlorophyll pigments were modeled into the density in several steps, which were interspersed by rigid-body refinements. In the first step, four inner-ring α helices (modeled as poly-alanine, except for a single histidine kept to facilitate the correct positioning of Bchl a) (5) were fitted into the best, elongated stretches of the density surrounding the RC. One of these helices (marked as W in Fig. 2C) was

substantially out of rank with the others. New maps were calculated and additional inner-ring helices and some bacteriochlorophylls (represented by bacteriochlorin macrocycles, i.e., Bchl a that lack phytol chains) were located. At this point, it was clear that the inner ring was composed of 16 α helices whose arrangement in the membrane plane deviates substantially from an exact circle. When all the inner-ring helices were modeled, the improved electron density allowed fitting of the outer-ring helices and remaining bacteriochlorins. However, only 15 stretches of density in the outer ring could be fitted with α helices; there was no density for the putative

16th α helix opposite the “misoriented” inner-ring helix W. Efforts to refit helix W to force its orientation to be more in rank with the other inner-ring α helices were unsatisfactory, because the initial density still remained while density for the new position was very poor.

It should be emphasized that, at this resolution, electron density shows only gross structural features. It is not possible to locate the LH1 carotenoid molecules or the phytol chains of the bacteriochlorophylls, the macrocycles of which are positioned with low accuracy. The final model, built with this bootstrapping approach, is shown in Fig. 2, B and C. Figure 3 shows the crystal packing of the RC-LH1 core complex viewed in an orientation parallel to the membrane plane in which this complex naturally resides. The main crystal contacts are approximately along the RC axis, which coincides with the a axis of the crystal lattice. Table 1 summarizes the diffraction data and refinement statistics.

At 4.8 Å resolution, the LH1 complex from *Rps. palustris* is seen to surround the RC with noncircular topology and an incomplete double ring of α helices. The elliptical LH1 complex has dimensions (measured as the distance between the centers of the opposite helices) of ~ 110 Å by ~ 95 Å for the outer ring, formed by the β -apoproteins. The longest dimension of the inner LH1 ellipsoid, formed by the α -apoproteins, is ~ 78 Å between the centers of the helices, which allows the RC (whose longest dimension in the membrane plane is ~ 70 Å) to be accommodated. The orientation of the long axis of the LH1 ellipse coincides with the long “axis” of the RC, so that the LH1 structure appears to be wrapped tightly around the RC.

The structure reveals a second distinctive feature at the location of helix W, where the regular LH1 structure with its repeating α - and β -apoprotein units is interrupted. The elliptical LH1 structure has a unique orientation with respect to the RC (Fig. 2C). Both

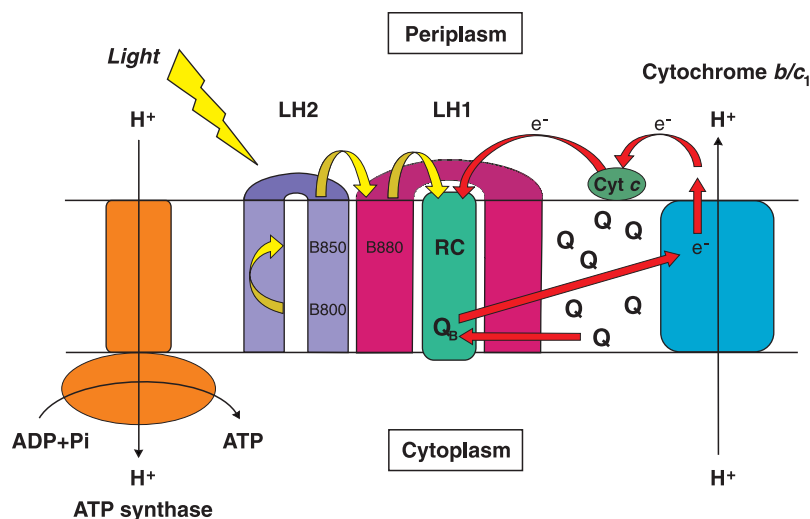


Fig. 1. A representation of the major membrane proteins involved in the light reactions of purple bacterial photosynthesis. Photon energy (yellow arrows) captured by the Bchl a pigments (labeled B800 and B850 to indicate the approximate wavelength in nanometers of maximal absorption) in the antenna LH2 (purple) is passed to the LH1 Bchl a (B880, red, which also acts as a light-harvester), and then to a pair of Bchl a molecules (not shown) in the RC. Electron flow (red arrows) occurs across the photosynthetic membrane from Bchl a , which is oxidized, to a primary electron acceptor, ubiquinone (UQ_A , not shown), which is reduced. Subsequently, the electron is transferred from UQ_A to the secondary electron acceptor ubiquinone (UQ_B , shown here as Q_B). A second RC turnover results in the complete reduction of UQ_B^- to UQ_BH_2 . The fully reduced UQ_BH_2 is replaced in the RC with an oxidized ubiquinone (shown as Q) and passes its electrons to the next redox component in the cyclic electron transport path, the cytochrome b/c_1 complex (blue) (75). Electrons (e^-) are returned to the RC through cytochrome c (Cyt c). A transmembrane proton gradient is established and drives ATP synthase (orange), producing ATP. ADP+Pi, adenosine diphosphate and inorganic phosphate.

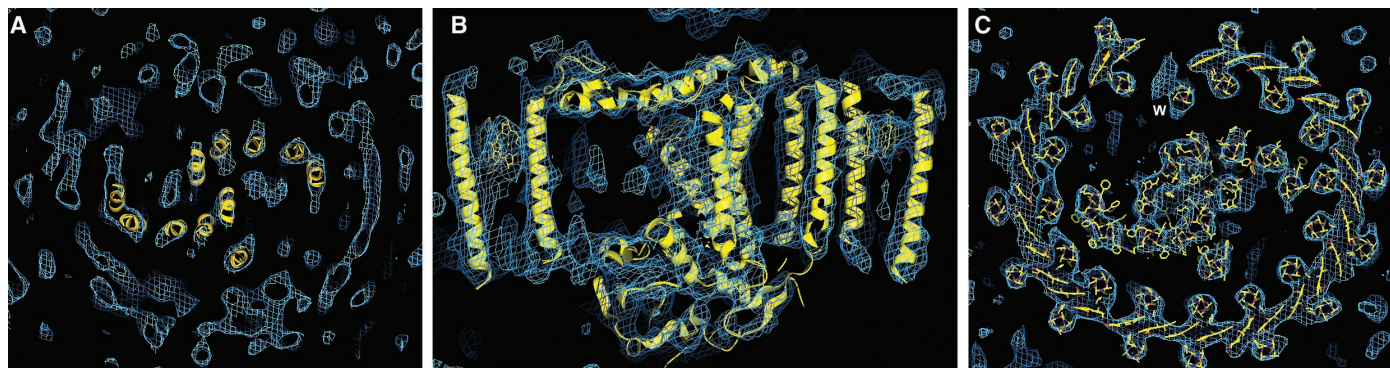


Fig. 2. Electron density ($2mF_o - DF_c$) maps (1.0σ contoured) for the RC-LH1 core complex. (A) First map calculated after MR with the RC model represented by ribbonlike transmembrane α helices (pigments are removed for clarity). (B) Final density with the core structure

(yellow) included in ribbon representation; view is parallel to the membrane plane. (C) Final map viewed along the RC’s pseudotwofold-axis with the final model of the core structure within the electron density.

the break of the outer ring of β -apoprotein helices and helix W of the LH1 complex are positioned on the opposite side of the RC with respect to the single transmembrane helix of the RC H subunit, which itself breaks the overall twofold symmetry of the RC. The W helix is therefore located next to the groove in the RC through which the tail of the secondary electron acceptor ubiquinone (UQ_B) projects into the membrane lipid phase. Figure 4, A and B, shows the core complex with the UQ_B (shown as Q_B) in its usual proximal position in the RC (4, 26, 27). The hydrophobic tail of UQ_B points toward the gap in the LH1 complex next to the W helix, strongly suggesting that this helix forms part of a gate through which UQ_BH_2 can move from the RC into the membrane lipid phase outside the LH1 complex. It further suggests that the location of helix W may play a major role in the unique positioning of the RC within the RC-LH1 complex, in order to facilitate this movement. The location of the single transmembrane α helix of the H subunit of the RC indicates that this helix could also play a critical role in the orientation of the RC within the LH1 complex.

In contrast, an 8.5 Å resolution, electron microscopy (EM) projection structure of the LH1 complex from *R. rubrum* (9) showed a circularly symmetrical structure composed of 16 subunits, interpreted as $\alpha\beta$ -heterodimers with their associated bacteriochlorophylls. The outside diameter of the ring was measured as 116 Å (similar to the longest outside dimension in this core complex structure). The LH1 complexes used in that study were reconstituted from detergent-solubilized $\alpha\beta$ -apoproteins and did not contain RCs, although the inside diameter of the ring (68 Å) was large enough to accommodate an RC. Subsequent low-resolution EM and atomic force microscopy (AFM) studies of intact RC-

LH1 complexes have shown an LH1 ring that surrounds the RC (10, 11, 13), with similar overall size and shape to that seen in the 8.5 Å resolution EM projection structure. However, other experiments have suggested that the LH1 ring of the core complex may not be fully closed and indeed may contain fewer than 16 subunits (14). A recent cryo-EM study of 2D crystals of RC-LH1 complexes from *R. rubrum*, also at 8.5 Å resolution, showed that although the LH1 rings are closed and composed of 16 identical subunits, their overall topology may be less restrained (10), with some complexes showing substantial deviation from circular symmetry. The observed variation was attributed to the flexibility of the complex and to the influence of the different crystal packing forces on the overall shape of the complex. Most recently, 10 Å resolution AFM images of core complexes in native membranes from *Rps. viridis* have shown that LH1 is a closed ellipsoid of 16 subunits, with the average long and short

dimensions of the ellipsoid estimated as 104 Å and 98 Å, respectively (28). These numbers are in good agreement with those obtained from the crystal structure, although the low resolution of the AFM images prevents a visualization of any dislocation in the LH1 ring structure. These experiments have also shown that the LH1 subunits rearrange into a circle after removal of the RC from the core complex. These AFM studies of core complexes in their native membranes show that the elliptical structure for the RC-LH1 complex from *Rps. palustris* observed in the crystalline state also indicates its *in vivo* condition.

The presence of helix W poses the question of whether it is a 16th α -apoprotein in the LH1 inner ring or a part of a PufX-like protein incorporated into the LH1 complex to facilitate the gating of the ubiquinone exchange. In *Rb. sphaeroides* and *Rb. capsulatus*, photosynthetic growth requires the presence of the 70-amino acid PufX protein, which is essential to promote an efficient

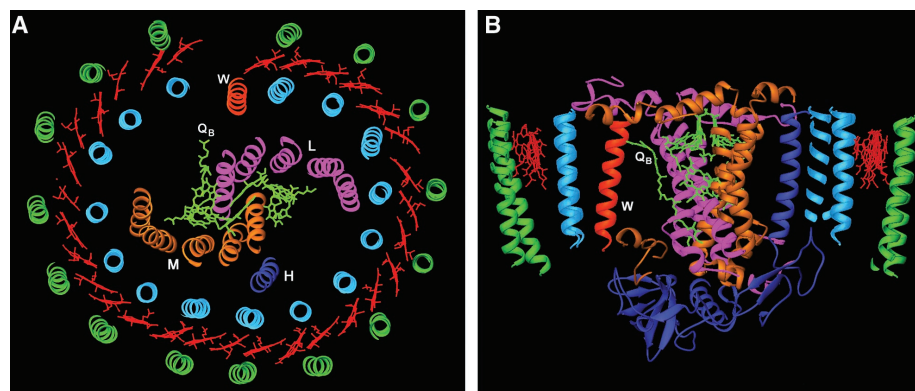


Fig. 4. Schematic model of the RC-LH1 core complex with the transmembrane helices represented by ribbons and the bacteriochlorophylls and bacteriopheophytins represented by their respective macrocycles, drawn with the program RIBBONS (30). (A) View of the complex perpendicular to the membrane plane and approximately along the pseudo-twofold axis of the RC. The pseudo-twofold axis relating L and M subunit helices of the RC does not relate RC helix H to helix W, and these two helices are inclined at different angles to this axis. (B) Narrow section of the complex viewed parallel to the membrane plane.

Table 1. Data collection and refinement statistics for the RC-LH1 core complex from *Rps. palustris*. $R_{\text{merge}} = (\sum |I - \langle I \rangle|) / (\sum I)$, where $\langle I \rangle$ is the average intensity of multiple measurements. R factor and $R_{\text{free}} = (\sum |F_o - F_c|) / (\sum |F_o|)$, where F_c and F_o are the calculated and observed structure factors, respectively.

Data collection (all data)	
Space group	P1
Resolution range (Å)*	60 to 4.8 (4.97 to 4.80)
No. of unique reflections/total	18,335/37,214
Mean $I/\sigma(I)$ *	8.3 (1.1)
Completeness (%)*	97.3 (83.4)
R_{merge} (%)*	8.6 (72.1)
Rigid-body refinement	
No. of reflections used†	17,391
R factor (%)	46.3
R_{free} (%)	48.4

*The numbers in parentheses are for the outer-resolution shell.

†This number does not include 5.15% of all available structure factors that were randomly chosen for calculation of R_{free} .

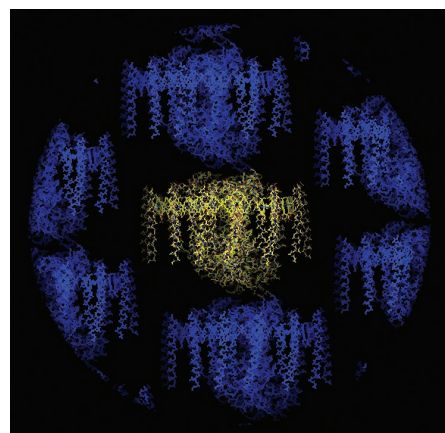


Fig. 3. Crystal packing of the RC-LH1 core complex (yellow) viewed parallel to the membrane plane; all neighboring molecules are colored blue.

REPORTS

ubiquinone/ubiquinol exchange between the RC and cytochrome *b/c*₁ (12, 17–20). Biochemical studies on these systems have shown that PufX is present in the RC-LH1 complex in a 1:1 stoichiometry with the RC and that it has a strong tendency to interact with the LH1 α -polypeptide (17). There is evidence that PufX is involved directly in the supramolecular organization of the photosynthetic system, prevents LH1 from completely encircling the RC, and perhaps induces a specific orientation of the RC inside the LH1 complex (29).

An equivalent gene for the PufX protein has not been identified in the *Rps. palustris* genome. This is not unexpected, because the PufX protein sequences, even for two such closely related species as *Rb. sphaeroides* and *Rb. capsulatus*, show only 23% identity (18); even for the α -helical membrane-spanning core region of PufX sequences, the identity is only 38%. In order to identify helix W, we performed matrix-assisted laser desorption/ionization–time-of-flight mass spectrometry analysis on purified RC-LH1 core complexes. In addition to the expected α - and β -apoproteins and the L, M, and H subunits of the RC, this revealed the presence of a protein of mass 10,707 D. So far, this protein appears to be N-terminally blocked and has resisted attempts to sequence it. There are more than 10 candidate genes in the *Rps. palustris* genome that could encode for putative membrane proteins of this mass. Efforts to identify the W gene are continuing.

References and Notes

1. R. van Grondelle, J. P. Dekker, T. Gillbro, V. Sundstrom, *Biochim. Biophys. Acta Bioenergetics* **1187**, 1 (1994).
2. R. J. Cogdell *et al.*, *J. Bacteriol.* **181**, 3869 (1999).
3. J. Deisenhofer, O. Epp, K. Miki, R. Huber, H. Michel, *Nature* **318**, 618 (1985).
4. G. Fritzsche, J. Koepke, R. Diem, A. Kuglstatler, L. Baciou, *Acta Crystallogr.* **D58**, 1660 (2002).
5. G. McDermott *et al.*, *Nature* **374**, 517 (1995).
6. M. Z. Papiž, S. M. Prince, T. Howard, R. J. Cogdell, N. W. Isaacs, *J. Mol. Biol.* **326**, 1523 (2003).
7. J. P. Abrahams, A. G. W. Leslie, R. Lutter, J. E. Walker, *Nature* **370**, 621 (1994).
8. S. Iwata *et al.*, *Science* **281**, 64 (1998).
9. S. Karrasch, P. A. Bullough, R. Ghosh, *EMBO J.* **14**, 631 (1995).
10. S. J. Jamieson *et al.*, *EMBO J.* **21**, 3927 (2002).
11. T. Walz, S. J. Jamieson, C. M. Bowers, P. A. Bullough, C. N. Hunter, *J. Mol. Biol.* **282**, 833 (1998).
12. T. Walz, R. Ghosh, *J. Mol. Biol.* **265**, 107 (1997).
13. A. Gall, thesis, University of Glasgow, UK (1994).
14. C. Jungas, J. L. Ranck, J. L. Rigaud, P. Joliet, A. Vermiglio, *EMBO J.* **18**, 534 (1999).
15. C. C. Moser *et al.*, *Adv. Protein Chem.* **63**, 71 (2003).
16. R. J. Cogdell *et al.*, *Photosynth. Res.* **48**, 55 (1996).
17. P. A. Recchia *et al.*, *Biochemistry* **37**, 11055 (1998).
18. P. S. Parkes-Loach *et al.*, *Biochemistry* **40**, 5593 (2001).
19. W. P. Barz *et al.*, *Biochemistry* **34**, 15235 (1995).
20. W. P. Barz *et al.*, *Biochemistry* **34**, 15248 (1995).
21. T. G. Lilburn, C. E. Haith, R. C. Prince, J. T. Beatty, *Biochim. Biophys. Acta* **1100**, 160 (1992).
22. P. McGlynn, C. N. Hunter, M. R. Jones, *FEBS Lett.* **349**, 349 (1994).
23. P. McGlynn, W. H. J. Westerhuis, M. R. Jones, C. N. Hunter, *J. Biol. Chem.* **271**, 3285 (1996).
24. Materials and methods are available as supporting material on Science Online.

25. K. E. McAuley *et al.*, *Proc. Natl. Acad. Sci. U.S.A.* **96**, 14706 (1999).
26. M. H. B. Stowell *et al.*, *Science* **276**, 812 (1997).
27. K. E. McAuley *et al.*, *Biochemistry* **39**, 15032 (2000).
28. S. Scheuring *et al.*, *Proc. Natl. Acad. Sci. U.S.A.* **100**, 1690 (2003).
29. R. N. Frese *et al.*, *Proc. Natl. Acad. Sci. U.S.A.* **97**, 5197 (2000).
30. M. Carson, *Methods Enzymol.* **277**, 493 (1997).
31. We thank A. Pitt for the mass spectrometry analyses and J. T. Beatty for bioinformatics. Coordinates have

been deposited with the Protein Data Bank (accession code 1PYH). Supported by grants from the Wellcome Trust and the Biotechnology and Biological Sciences Research Council.

Supporting Online Material

www.sciencemag.org/cgi/content/full/302/5652/1969/DC1

Materials and Methods
Figs. S1 to S5

7 July 2003; accepted 20 October 2003

Mono- Versus Polyubiquitination: Differential Control of p53 Fate by Mdm2

Muyang Li, Christopher L. Brooks, Foon Wu-Baer, Delin Chen, Richard Baer, Wei Gu*

Although Mdm2-mediated ubiquitination is essential for both degradation and nuclear export of p53, the molecular basis for the differential effects of Mdm2 remains unknown. Here we show that low levels of Mdm2 activity induce monoubiquitination and nuclear export of p53, whereas high levels promote p53's polyubiquitination and nuclear degradation. A p53-ubiquitin fusion protein that mimics monoubiquitinated p53 was found to accumulate in the cytoplasm in an Mdm2-independent manner, indicating that monoubiquitination is critical for p53 trafficking. These results clarify the nature of ubiquitination-mediated p53 regulation and suggest that distinct mechanisms regulate p53 function in accordance with the levels of Mdm2 activity.

The p53 tumor suppressor protein induces cell growth arrest, apoptosis, and senescence in response to various types of stress (1). In unstressed cells, p53 is maintained at low levels by the action of Mdm2, an oncogenic E3 ligase. Numerous studies indicate that the ubiquitin ligase activity of Mdm2 is essential for both degradation and nuclear export of p53 (2–12). We investigated the molecular basis for the differential effects of Mdm2 on p53 fate.

To examine whether Mdm2 alone catalyzes polyubiquitination (conjugation with a polymeric ubiquitin chain) or only monoubiquitination (conjugation with a ubiquitin monomer at one or multiple sites) of p53, we performed an in vitro ubiquitination assay using purified components (fig. S1A). Incubation of Flag-p53 with glutathione *S*-transferase (GST)–Mdm2 in the presence of E1, E2, and ubiquitin generated ubiquitin-conjugated forms of p53 (fig. S1B). We then tested whether Mdm2 induced the same effect with a mutant form of ubiquitin (UbK0), in which all seven lysine residues (K6, K11, K27, K29, K33, K48, and K63) were replaced by arginine (fig. S1C). Because this

mutant lacks potential sites for polyubiquitination, it should support only monoubiquitination. The patterns of p53-ubiquitin conjugates generated by wild-type and mutant ubiquitin were indistinguishable (fig. S1B), indicating that Mdm2 primarily catalyzes monoubiquitination of p53 at multiple sites under these conditions.

Yet, in contrast to these results, we and others have previously demonstrated that Mdm2 alone is apparently sufficient to induce polyubiquitination of p53 when in vitro–translated p53 polypeptides are used as substrates for in vitro ubiquitination (11, 13–17). To test the possibility that the outcome (mono versus poly) of Mdm2-mediated ubiquitination is influenced by the enzyme: substrate ratio, we prepared ubiquitination reactions containing a constant amount of recombinant p53 and varying amounts of Mdm2 (Fig. 1A). Monoubiquitination of p53 was observed when the Mdm2:p53 ratio was low, whereas slower-migrating, polyubiquitinated forms of p53 were observed when the Mdm2:p53 ratio reached 3.6 or higher. Because the polyubiquitination-defective ubiquitin mutant (UbK0) only supported the faster-migrating, monoubiquitinated forms of p53 (Fig. 1B), the higher-molecular-weight ubiquitin conjugates clearly represent polyubiquitinated p53. These data indicate that Mdm2 catalyzes both mono- and polyubiquitination in a dosage-dependent manner.

Institute for Cancer Genetics and Department of Pathology, College of Physicians & Surgeons, Columbia University, 1150 St. Nicholas Avenue, New York, NY 10032, USA.

*To whom correspondence should be addressed. E-mail: wg8@columbia.edu